Yap and Taz play a crucial role in neural crest-derived craniofacial development

Jun Wang[1,5,*], Yang Xiao[1,2], Chih-Wei Hsu[1], Idaliz M. Martinez-Traverso[1,8], Min Zhang[1], Yan Bai[1], Mamoru Ishii[3], Robert E. Maxson[3], Eric N. Olson[4], Mary E. Dickinson[1,5,6,8], Joshua D. Wythe[1,5,6], and James F. Martin[1,2,5,6,7,8*]

[1]Department of Molecular Physiology and Biophysics, Baylor College of Medicine, One Baylor Plaza, Houston, TX 77030, USA. [2]Institute of Biosciences and Technology, Texas A&M Health Science Center, Houston, TX 77030, USA. [3]Department of Biochemistry and Molecular Biology, USC/Norris Comprehensive Cancer Center, Keck School of Medicine, University of Southern California, Los Angeles, CA 90033, USA. [4]Department of Molecular Biology, University of Texas Southwestern Medical Center, Dallas, TX 75390, USA. [5]Cardiovascular Research Institute, Baylor College of Medicine, One Baylor Plaza, Houston, TX 77030, USA. [6]Program in Developmental Biology, Baylor College of Medicine, One Baylor Plaza, Houston, TX 77030, USA. [7]Texas Heart Institute, Houston, TX 77030, USA. [8] Interdepartmental Graduate Program in Translational Biology and Molecular Medicine

***Corresponding author:** James F. Martin or Jun Wang, Department of Molecular Physiology and Biophysics, Baylor College of Medicine, 1 Baylor Plaza, Houston, TX 77030, USA; Phone: 713-798-5931; E-mail: jfmartin@bcm.edu (J. F. Martin); E-mail: junw@bcm.edu (J. Wang)

Key words: Yap and Taz, cranial neural crest, craniofacial development

List of abbreviations used

AHA, American Heart Association; ARS, Axenfeld-Rieger syndrome; CFL1, cofilin 1; ChIP, chromatin immunoprecipitation; CKO, conditional knock out; CNC, cranial neural crest; CVH, cerebellar vermis hypoplasia; DAPI, diamidino-2-phenylindole; dUTP, deoxynucleotidyl transferase; DWM, Dandy-Walker malformation; FACS, fluorescence-activated cell sorting; Fox, forkhead box; GFP, green fluorescent protein; H&E, hematoxylin and eosin; NC, neural crest; OPT, optical projection tomography; PBS, phosphate buffered saline; Pdgfb, Platelet-derived growth factor b; PFA, paraformaldehyde; pYAP, phosphorylated Yap; RNA-Seq, RNA-sequencing; SDG, Scientist Development Grant; SFRP, secreted Frizzled-related protein; SMA, smooth muscle actin; TEA, transcriptional enhancer activator; Tead, TEA domain; TUNEL, terminal deoxynucleotidyl transferase nick end labeling.

ABSTRACT

The role of the Hippo signaling pathway in cranial neural crest (CNC) development is poorly understood. We used the *Wnt1*^{Cre} and *Wnt1*^{Cre2SOR} drivers to conditionally ablate both *Yap* and *Taz* in the CNC of mice. When using either Cre driver, *Yap* and *Taz* deficiency in the CNC resulted in enlarged, hemorrhaging branchial arch blood vessels and hydrocephalus. However, *Wnt1*^{Cre2SOR} embryos had an open cranial neural tube phenotype that was not evident in *Wnt1*^{Cre} embryos. In O9-1 CNC cells, the loss of *Yap* and *Taz* impaired smooth muscle cell differentiation. RNA-sequencing data indicated that Yap and Taz regulate genes encoding Fox transcription factors, specifically *Foxc1*. Proliferation was reduced in the branchial arch mesenchyme of *Yap* and *Taz* CNC conditional knockout (CKO) embryos. Moreover, *Yap* and *Taz* CKO embryos had cerebellar aplasia similar to Dandy Walker spectrum malformations observed in human patients and mouse embryos with mutations in *Foxc1*. In embryos and O9-1 cells deficient for *Yap* and *Taz*, *Foxc1* expression was significantly reduced. Analysis of *Foxc1* regulatory regions revealed a conserved recognition element for the Yap and Taz DNA binding co-factor Tead. ChIP-pcr experiments further supported the conclusion that *Foxc1* is directly regulated by the Yap/Tead complex. Our findings uncover important roles for *Yap* and *Taz* in CNC diversification and development.

INTRODUCTION

The neural crest (NC) is a migratory, multipotent cell population that originates in the embryonic dorsal neural tube. Developmental defects in NC formation result in numerous human congenital anomalies. Based on the site of origin, NC cells are divided into cranial, cardiac, and trunk populations, each of which has its own unique developmental potential. The cranial neural crest (CNC) ultimately diversifies into multiple cells types including neuronal, glial, cartilage, bone, and smooth muscle cells (Santagati and Rijli, 2003). Mutations in the genes required for CNC development are often associated with the pathophysiology of human congenital malformations (Acloque et al., 2009; Cordero et al., 2011), highlighting the clinical importance of understanding the molecular mechanisms governing CNC development. Much effort has been expended interrogating the gene regulatory networks underlying NC development (Sauka-Spengler and Bronner-Fraser, 2008). Major signaling pathways, including Wnt, Fgf, Bmp, and Notch signaling, have been shown to play important roles in regulating NC induction, proliferation, and migration (Sela-Donenfeld and Kalcheim, 1999; Garcia-Castro et al., 2002; Coles et al., 2004; Glavic et al., 2004; Carmona-Fontaine et al., 2008). However, the function of Hippo signaling in CNC development remains poorly understood.

Hippo signaling is a critical pathway that regulates organ size through the modulation of cell proliferation (Heallen et al., 2011). The key components of the Hippo signaling pathway are evolutionarily conserved. In mice, Mst1/2 (orthologous to *Drosophila melanogaster* Hpo) and Salv (orthologous to human WW45) form a complex that phosphorylates the kinases Lats 1/2 (orthologous to *Drosophila* Warts). Lats 1/2, in turn, phosphorylate the most downstream Hippo signaling components Yap and Taz, thus promoting their binding to 14-3-3 proteins and inhibiting them from shuttling into the nucleus. In the absence of Hippo signaling repressive activity, Yap and Taz localize in the nucleus and partner with transcription factors, such as transcriptional enhancer activator (TEA) domain (Tead) family members, to promote gene programs favoring proliferation. Recently, familial studies have shown that heterozygous nonsense mutations in *YAP1* are associated with variable phenotypes in the affected families, including orofacial clefting and intellectual disability (Williamson et al., 2014). However, the mechanisms underlying these phenotypic alterations remain unclear.

In this study, we investigated *Yap* and *Taz* function in the CNC. Using two *Wnt1* Cre drivers, we uncover important functions *Yap* and *Taz* CNC proliferation and subsequent CNC differentiation.

RESULTS

Yap and *Taz* deletion in CNC-derived cells results in embryonic lethality

To determine the function of *Yap* and *Taz* in the CNC, we generated compound *Yap* and *Taz* conditional mutants by using conditional null alleles and the CNC *Wnt1*^{Cre} and *Wnt1*^{Cre2SOR} drivers. We collected embryos at multiple developmental stages to analyze the morphogenesis of several CNC-derived structures. Importantly, the *Wnt1*^{Cre} driver (Chai et al., 2000) has been shown to induce ectopic expression of *Wnt1*, leading to defects in midbrain development, whereas the *Wnt1*^{Cre2SOR} driver does not have these issues (Lewis et al., 2013).

We first evaluated embryos in which *Yap* and *Taz* were deleted using the *Wnt1*^{Cre} driver. In control embryos, phosphorylated Yap (pYAP)—a readout for Hippo signaling activity—was present in CNC-derived cells, such as mandibular mesenchymal cells (Fig. 1A,B). However, in *Wnt1*^{Cre}; *Yap*; *Taz* double conditional knockout *(*dCKO) embryos, the level of pYAP was dramatically reduced in CNC-derived cells, but unchanged in non–CNC-derived cells such as endothelium (Fig. 1C,D). These data indicated that the *Wnt1*^{Cre} driver efficiently inactivated *Yap* and *Taz* in CNC-derived cells. Among the different mutant genotypes, both *Wnt1*^{Cre}; *Yap*$^{f/f}$; *Taz*$^{f/+}$ and *Wnt1*^{Cre}; *Yap*; *Taz* dCKO were embryonic lethal at embryonic day 10.5 (E10.5) (Table S1). Mutant embryos with the reciprocal genotype of *Wnt1*^{Cre}; *Yap*$^{f/+}$; *Taz*$^{f/f}$ displayed lethality over a wide range of developmental time points, from E14.5 to postnatal week 8 (Table S1).

In addition, we used the *Wnt1*^{Cre2SOR} driver (Lewis et al., 2013) to inactivate *Yap* and *Taz* in CNC. Similar to *Wnt1*^{Cre} embryos, lethality was observed at E10.5 in both *Wnt1*^{Cre2SOR}; *Yap*$^{f/f}$; *Taz*$^{f/+}$ and *Wnt1*^{Cre2SOR}; *Yap*; *Taz* dCKO embryos, whereas *Wnt1*^{Cre2SOR}; *Yap*$^{f/+}$; *Taz*$^{f/f}$ embryos survived until E15.5, the latest developmental stage examined in this study (Table S2). Together, our findings indicate that embryos with *Yap* and *Taz* compound loss of function or *Yap* deletion with *Taz* haploinsufficiency in the CNC exhibit early embryonic lethality, whereas embryos with *Taz* deletion and *Yap* haploinsufficiency in the CNC survive until later developmental stages.

Yap and *Taz* deletion in *Wnt1*^{Cre} and *Wnt1*^{Cre2SOR} embryos results in similar vascular defects, but distinct neural tube phenotypes

No obvious craniofacial morphologic defects were observed in *Yap* and *Taz* compound mutants at E9.5. At E10.5, neither control embryos, including *Yap* and *Taz* compound heterozygous embryos and embryos without *Wnt1*^{Cre} (Fig. S1A-C), nor *Wnt1*^{Cre}; *Yap*$^{f/+}$; *Taz*$^{f/f}$

embryos (Fig. S1D-F) displayed any obvious craniofacial defects. The *Wnt1*^{Cre}; *Yap*$^{f/f}$; *Taz*$^{f/+}$ (Fig. S1G-I) and *Wnt1*^{Cre}; *Yap*; *Taz* dCKO (Fig. S1J-L,P-R) embryos survived until E10.5 and showed disrupted craniofacial structures, including enlarged blood vessels in the branchial arch and hemorrhage in the forebrain and mandible at E10.5.

Similar to *Wnt1*^{Cre}*; Yap; Taz* mutant embryos, E10.5, lethality was observed in *Wnt1*^{Cre2SOR}; *Yap*; *Taz* dCKO (Fig. 2A-D) and *Wnt1*^{Cre2SOR}; *Yap*$^{f/f}$; *Taz*$^{f/+}$ (Fig. 2M-P) embryos. The E10.5 mutant embryos exhibited disrupted craniofacial structures, including blood vessel enlargement and hemorrhage, which are phenotypes we observed in *Wnt1*^{Cre} compound mutant embryos. These early CNC phenotypes were not observed in *Wnt1*^{Cre2SOR}; *Yap*$^{f/+}$; *Taz*$^{f/f}$ embryos that have one functional copy of Yap or controls (Fig. 2E-L). *Wnt1*^{Cre2SOR} compound mutant embryos lacked any obvious morphologic defects at E9.5. Notably, both E10.5 *Wnt1*^{Cre2SOR}; *Yap*$^{f/f}$; *Taz*$^{f/+}$ (Fig. 2P,p) and *Wnt1*^{Cre2SOR}; *Yap*; *Taz* dCKO (Fig. 2D,R) embryos had neural tube defects, which is one of the most common human birth defects. At E10.5, all (14/14) *Wnt1*^{Cre2SOR}; *Yap*; *Taz* dCKO embryos displayed open anterior neural tubes (Fig. 2D,R), and most (7/11) *Wnt1*^{Cre2SOR}; *Yap*$^{f/f}$; *Taz*$^{f/+}$ embryos presented with less severe, but still abnormal, anterior neural tube morphology (Fig. 2P,p). Neural tube defects were not observed in any of the *Yap*; *Taz* compound mutant embryos generated using *Wnt1*^{Cre} (Fig. S1).

Histologic analysis indicated that, compared to control embryos (Fig. 3A-D; Fig. S2A-C), both *Wnt1*^{Cre}; *Yap*; *Taz* dCKO (Fig. 3E-L; Fig. S2D-F) and *Wnt1*^{Cre}; *Yap*$^{f/f}$; *Taz*$^{f/+}$ (Fig. 3M-P; Fig. S2 G-I) embryos had enlarged blood vessels. Moreover, the mandibular mesenchyme was disorganized in *Wnt1*^{Cre}; *Yap*; *Taz* dCKO (Fig. 3G,H) and *Wnt1*^{Cre}; *Yap*$^{f/f}$; *Taz*$^{f/+}$ (Fig. 3O,P) embryos. The sparse mesenchyme in the mandible suggests that there are fewer pericytes to be recruited from the surrounding mesenchyme due to lack of in *Yap* and *Taz* in CNC-derived tissues, thus deficient support from the blood vessels surrounding cells likely caused hemorrhage in mutants.

Yap and *Taz* deletion causes severe neural tube vessel regression

To more closely examine the hemangioma phenotype in the forebrain, branchial arch, and mandibular regions *in Wnt1*^{Cre}; *Yap*; *Taz* dCKO embryos, we performed whole mount immunofluorescence staining for CD31 (Pecam1, endothelial cell marker) and smooth muscle actin (SMA, a smooth muscle cell marker), followed by imaging with Lightsheet microscopy. In contrast to control embryos (Fig. 4A), the hemangiomas present in the branchial arch of *Wnt1*^{Cre}; *Yap*; *Taz* dCKO embryos are encapsulated by CD31-positive

endothelium (Fig. 4B). In addition, the results of three-dimensional rendering and maximum intensity projection of the branchial arch in a *Yap*; *Taz* dCKO embryo further supported that the vessels were wrapped around the hemangioma in the branchial arch of the *Yap*; *Taz* dCKO embryo (Fig. 4C). Similar endothelial-lined hemangiomas were also identified in the forebrain and mandibular regions in other dCKO embryos. Images of CD31 immunostaining also revealed abnormal vessel regression throughout the brain of *Wnt1*^{Cre}; *Yap*; *Taz* dCKO embryos. By comparing control embryos (Fig. 4D-F) with *Wnt1*^{Cre}*; Yap*$^{f/f}$*; Taz*$^{f/f}$ embryos (Fig. 4G-I), we detected several regions where vessel regression and/or disorganization was present in *Wnt1*^{Cre}*; Yap*$^{f/f}$*; Taz*$^{f/f}$ embryos (regions labeled as 1-4 in Fig. 4G-I), demonstrating that *Yap* and *Taz* within the CNC is required for normal vascularization of the early brain and mandibular region.

RNA-sequencing reveals genes regulated by the Hippo pathway in the CNC

Because the mandibular phenotype in *Yap*; *Taz* dCKO embryos appeared to be consistent in both CNC-specific Cre lines, we focused our attention on the molecular mechanism underlying the enlarged cranial and facial vessels. We performed RNA-sequencing (RNA-Seq) analysis by using mandibular RNA isolated from E10.5 *Wnt1*^{Cre}; *Yap*; *Taz* dCKO and control embryos. RNA-Seq analysis of the mandibular tissue from *Wnt1*^{Cre}; *Yap*; *Taz* dCKO embryos revealed efficient ablation of *Yap* and *Taz* (Fig. 5A). Among the differentially expressed genes, 355 were upregulated and 77 were downregulated (Fig. S3A). We noted that a large percentage of the differentially expressed genes (11%) were DNA binding factors (Fig. S3B).

Gene ontology analysis indicated that genes upregulated in *Wnt1*^{Cre}; *Yap*; *Taz* dCKO embryos are involved in regulating adherens junction formation, vasoconstriction, cytoskeleton, and positive regulation of endothelial cell migration (Fig. 5B). Genes downregulated in *Wnt1*^{Cre}; *Yap*; *Taz* dCKO embryos primarily function in cell proliferation, extracellular matrix organization, and vasculogenesis (Fig. 5C).

Among the downregulated genes, we identified those that negatively regulate the canonical Wnt signaling pathway, including the secreted Frizzled-related protein (SFRP) *Sfrp*2, a Wnt inhibitor that directly binds Wnt ligands (Ladher et al., 2000). Notably, *Wnt1*^{Cre}; *Yap*; *Taz* dCKO embryos had reduced *Foxc1* expression (Fig. 5D). *Foxc1* has been implicated in ocular and cerebellar malformations in human patients, as well as in vascular malformations in mice (Kume et al., 2001; Kume, 2009; Delahaye et al., 2012; Haldipur et al., 2014).

Among the transcripts upregulated in *Wnt1*^{Cre} *Yap; Taz* dCKO embryos, we identified genes encoding components of the Jak-Stat cascade, including *Jak3*, *Ptk2b*, *Stat3*, *Stat5a*, and *Stat5b* (Fig. 5D). Interestingly, Jak-Stat signaling controls organ size in *Drosophila*, much like the Hippo pathway. In vertebrates, the Jak-Stat pathway is involved in growth hormone signaling, although it is less clear what the predicted consequence of increased Jak-Stat levels would be during development. We also found that *Prospero Homeobox Protein 1* (*Prox1*) expression is upregulated in *Wnt1*^{Cre}; *Yap*; *Taz* dCKO embryos. *Prox1* encodes a transcription factor that is a master regulator of lymphatic endothelial cell specification and identity, and is essential for normal vascular development (Wigle and Oliver, 1999; Wigle et al., 2002; Johnson et al., 2008). Another upregulated vascular mitogen was *Platelet-derived growth factor b* (*Pdgfb*), which promotes the recruitment and proliferation of vascular cells (Yancopoulos et al., 2000). *Pdgfb* deficiency leads to reduced numbers of microvascular-associated pericytes in mouse embryos (Lindahl et al., 1997). *Wnt1*^{Cre}; *Yap*; *Taz* dCKO embryos also had upregulated expression of *Forkhead Box E1* (*Foxe1*), which has been implicated as a causative gene in human orofacial clefting (Moreno et al., 2009).

Yap and *Taz* regulate proliferation and apoptosis in the CNC

As indicated by our RNA-Seq data analysis (Fig. 5C), cell proliferation genes were downregulated in *Wnt1*^{Cre}; *Yap*; *Taz* dCKO embryos compared to control embryos. To evaluate differences in proliferation *in vivo*, we performed phospho-histone H3 (pHH3) immunofluorescence staining on sections from both E9.5 and E10.5 *Yap*; *Taz* dCKO and control embryos. The percentage of proliferating, pHH3-positive cells was lower in the mandible of *Wnt1*^{Cre}; *Yap*; *Taz* dCKO embryos (E9.5 Fig. 6C,D; E10.5 Fig. 6H,I) than in that of control embryos (E9.5 Fig. 6A,B; E10.5 Fig. 6F,G). Furthermore, quantification of pHH3-positive cells indicated that the rate of proliferation was significantly lower in *Wnt1*^{Cre}; *Yap*; *Taz* dCKO embryos than in control embryos at both E9.5 and E10.5 (Fig. 6E,J).

To further evaluate the role of the Hippo pathway in CNC cells, we used the O9-1 cell line for *in vitro* analyses. The O9-1 cell line is a stable, multipotent, mesenchymal CNC cell line, originally derived from *Wnt1*^{Cre}; R26R-green fluorescent protein (GFP)-expressing cells and can differentiate into multiple CNC-derivatives, including osteoblasts, chondrocytes, smooth muscle cells, and glial cells (Ishii et al., 2012). To examine cell proliferation in response to altered Hippo signaling, we used siRNA-mediated knockdown to reduce *Yap* and *Taz*, as well as *Lats1* and *Lats2*, levels in O9-1 cells, and performed pHH3 immunofluorescence staining to assess cell proliferation. The percentage of pHH3-positive

cells was decreased in cells treated with siRNA against *Yap* and *Taz* (Fig. 6L), but was increased in cells treated with siRNAs targeting *Lats1* and *Lats2* (Fig. 6M) compared to cells treated with control siRNA (Fig. 6K). Based on cell counting, the proliferation rate was significantly reduced in *Yap* and *Taz* knockdown cells but significantly increased in *Lats1* and *Lats2* knockdown cells when compared with control siRNA-treated cells (Fig. 6N).

Although cell proliferation was reduced in the mandible of *Wnt1*^{Cre}; *Yap*; *Taz* dCKO embryos, these mutant embryos showed no obvious defects in neural tube morphogenesis. We also evaluated cell proliferation in *Wnt1*^{Cre2SOR} *Yap*; *Taz* dCKO embryos, which did display neural tube closure defects (Fig. 2R). However, no obvious difference was detected in cell proliferation within the neural tube between *Wnt1*^{Cre2SOR} *Yap*; *Taz* dCKO and control embryos (Fig. S4). Moreover, when we performed immunofluorescence studies to evaluate the expression of the actin-severing protein cofilin 1 (CFL1), an important factor for neural tube closure, we found no obvious difference between *Wnt1*^{Cre2SOR} *Yap*; *Taz* dCKO and control embryos (Fig. S5).

Our RNA-Seq data indicated that the expression levels of negative regulators of apoptosis were lower in *Wnt1*^{Cre}; *Yap*; *Taz* dCKO embryos than in control embryos (Fig. 5C). To evaluate cell apoptosis *in vivo*, we performed terminal deoxynucleotidyl transferase (dUTP) nick end labeling (TUNEL) analysis in both E9.5 *Wnt1*^{Cre}; *Yap*; *Taz* dCKO mutant embryos and control embryos. Our TUNEL data indicated that cell apoptosis was significantly increased in E9.5 *Wnt1*^{Cre};*Yap*; *Taz* dCKO embryos compared to control embryos (Fig. 6O-S).

Yap and *Taz* promote smooth muscle differentiation

Our RNA-Seq data indicated that genes involved in vasculogenesis are downregulated in *Wnt1*^{Cre}; *Yap*; *Taz* dCKO embryos when compared with control embryos (Fig. 5C). Moreover, Lightsheet microscopy revealed severe vessel defects in *Wnt1*^{Cre}; *Yap*; *Taz* dCKO embryos than in control embryos (Fig. 4). A recent study indicated that *Yap* and *Taz* deficiency gives rise to smooth muscle differentiation defects partially derived from the CNC (Manderfield et al., 2015) . Given the similar vessel defects in *Wnt1*^{Cre}; *Yap*$^{f/f}$; *Taz*$^{f/+}$ embryos and *Wnt1*^{Cre}; *Yap*; *Taz* dCKO embryos, we hypothesized that *Yap* alone plays a critical role in the regulation of smooth muscle differentiation. Accordingly, we created a *Yap* null O9-1 cell line (*Yap* KO O9-1) by removing exon 3 of *Yap* using CRISPR/Cas9-mediated genome editing (the strategy is shown in Fig. 7A and details are provided in the Methods section). Compared to wild-type O9-1 cells, *Yap* KO O9-1 cells had diminished SMA protein

expression and Yap activity (Fig. 7B). SMA immunofluorescence indicated that under differentiation conditions (see Methods section), wild-type O9-1 cells gave rise to SMA-positive smooth muscle cells, but the ability of *Yap* KO O9-1 cells to generate SMA-positive cells was significantly diminished supporting the idea that Yap plays the predominant function is SMC differentiation perhaps because it is more highly expressed in CNC (Fig. 7C-E).

Hydrocephalus in *Yap*$^{f/+}$; *Taz*$^{f/f}$ CKO embryos

Although *Wnt1*^{Cre}; *Yap*$^{f/+}$; *Taz*$^{f/f}$ and *Wnt1*^{Cre2SOR}; *Yap*$^{f/+}$; *Taz*$^{f/f}$ embryos did not show any obvious defects before E10.5 (Fig. 2; Fig. S1), they developed hydrocephalus at later stages (Fig. S6E-G; Fig. S7D-F). Hydrocephalus is mainly characterized by the abnormal widening of brain spaces caused by the excessive accumulation of cerebrospinal fluid, which places harmful pressure on the surrounding tissues of the brain. Figure S6E-G shows a representative example of an E12.5 *Wnt1*^{Cre}; *Yap*$^{f/+}$; *Taz*$^{f/f}$ embryo that had severe hydrocephalus in the hindbrain. In addition, in the sagittal sections of control embryos (Fig. S6D,d), the cerebellum structure is clearly visible, whereas it is missing in the *Wnt1*^{Cre}; *Yap*$^{f/+}$; *Taz*$^{f/f}$ embryos (Fig. S6H,h). The hydrocephalus phenotype was detected as early as E11 in *Wnt1*^{Cre}; *Yap*$^{f/+}$; *Taz*$^{f/f}$ embryos, but it was not observed in either *Wnt1*^{Cre}; *Yap*$^{f/f}$; *Taz*$^{f/+}$ or *Wnt1*^{Cre}; *Yap*; *Taz* dCKO embryos, most likely because of their lethality at E10.5. Moreover, *Wnt1*^{Cre}; *Yap*$^{f/f}$ embryos at E11 also had severe hydrocephalus (Fig. S8M-P) when compared to controls (Fig. S8I-L). *Wnt1*^{Cre2SOR}; *Yap*$^{f/+}$; *Taz*$^{f/f}$ embryos at E12.5 presented more severe hydrocephalus (Fig. S7D-F) than that in *Wnt1*^{Cre}; *Yap*$^{f/+}$; *Taz*$^{f/f}$ embryos in the hindbrain region and forebrain region. Notably, our RNA-Seq data (Fig. 5) suggested that genes required for forebrain and hindbrain morphogenesis were regulated by *Taz* and *Yap*, such as *Foxc1*. *Foxc1* loss of function also leads to hydrocephalus in mice (Kume et al., 1998).

***Yap* and *Taz* regulate Fox genes**

Our RNA-Seq data indicated that *Yap* and *Taz* modulated the expression of multiple members of the winged-helix/forkhead box (*Fox*) transcription factor family, including the upregulation of *Foxe1*, *Foxh1*, *Foxj1*, and *Foxo3*, as well as the downregulation of *Foxc1* (Fig. 5D). We focused on *Foxc1* in part because its expression was reduced in *Wnt1*^{Cre}; *Yap*; *Taz* dCKO embryos and Yap and Taz are thought to be transcriptional activators. Indeed Yap ChIP Seq data showed that genome wide Yap peaks are enriched in active chromatin regions

as defined by H3K27Ac chromatin marks (Morikawa et al., 2015). We reasoned that downregulated genes were more likely to be direct Yap/Taz target genes. Moreover, *Foxc1* is the gene mutated in the congenital hydrocephalus mouse mutant (Kume et al., 1998).

Immunohistochemistry data indicated that Foxc1 is normally expressed in the majority of the epithelial and mesenchymal cells in the mandible (sagittal view in Fig. 8A-b2; coronal view in Fig. S9A-b2), yet Foxc1 expression was missing or reduced in the majority of mesenchymal cells and unchanged in the mandibular epithelial cells in *Wnt1*^{Cre}; *Yap*; *Taz* dCKO embryos (sagittal view in Fig. 8C-d2; coronal view in Fig. S9C-d2). On the basis of cell counting, the number of Foxc1-positive cells was significantly lower in the *Wnt1*^{Cre}; *Yap*; *Taz* dCKO mandible than in the control mandible ($p<0.01$, Fig. 8E). Furthermore, Foxc1 immunofluorescence staining indicated that Foxc1 expression was significantly lower in *Yap* knockout; *Taz* knockdown O9-1 cells (Fig. 8G) than in wild-type O9-1 cells (Fig. 8F) ($p<0.05$, Fig. 8H). Western blot analysis of Foxc1 further indicated that Foxc1 expression was decreased in response to the decrease in Yap and Taz expression levels (Fig. 8I).

Importantly, we identified a conserved binding site for Tead, the Yap and Taz cofactor, in *Foxc1* (Fig. 8J). Craniofacial cis-regulatory landscapes were recently studied by deep-sequencing of transposase-accessible chromatin (ATAC-seq) in human and chimpanzee cranial neural crest cells (Prescott et al., 2015). Bioinformatic analysis of these data set (accession no. GSE70751) revealed increased chromatin accessibility in a region located upstream of the 5' UTR of *FOXC1*. Significantly, this putative enhancer region contained a potential TEAD DNA-binding element (Fig. 8J). The TEAD binding element was confirmed by chromatin immunoprecipitation (ChIP) PCR in murine embryonic facial tissue using an anti-Yap antibody, indicating that a Yap-Tead complex directly binds to *Foxc1* chromatin during embryonic facial morphogenesis (Fig. 8K).

DISCUSSION

During normal development, regeneration, and cancer progression, Hippo signaling inhibits proliferation while promoting apoptosis. Here, we show that, during craniofacial development, *Yap* and *Taz*, the final downstream effectors of Hippo signaling, regulate multiple events in CNC diversification including vasculogenesis, smooth muscle differentiation, cerebellar development, and neural tube closure. Furthermore, our data indicate that *Foxc1* is an important downstream target of Yap and Taz. Significantly, *Foxc1* loss of function in mouse embryos phenocopies several of the morphological defects present in *Yap* and *Taz* mutant embryos.

Overlapping functions for *Yap* and *Taz* during craniofacial development

Using either a $Wnt1^{Cre}$ or $Wnt1^{Cre2SOR}$ driver, *Yap* and *Taz* conditional CNC mutants presented with disrupted craniofacial vascular development and hemorrhage. We also observed hydrocephalus in $Yap^{f/+}$; $Taz^{f/f}$ mutants established by using both Cre drivers, at later embryonic stages. It is most likely that *Yap* and *Taz* have redundant functions when they are co-expressed, but at earlier developmental stages, *Taz* expression is lower than that of *Yap*. Interestingly, we did observe a phenotypic difference in embryos when we deleted *Yap* and *Taz* using the two Cre drivers. Deleting *Yap* and *Taz* with the $Wnt1^{Cre2SOR}$ driver resulted in anterior neural tube closure defects at E10.5, whereas $Wnt1^{Cre}$; $Yap^{f/f}$; $Taz^{f/+}$ and $Wnt1^{Cre}$; *Yap*; *Taz* dCKO embryos showed no neural tube closure defects. $Wnt1^{Cre}$ directs ectopic Wnt1 activity in the midbrain, whereas $Wnt1^{Cre2SOR}$ has normal Wnt1 activity in the midbrain (Lewis et al., 2013). Because Wnt signaling is known to stabilize Yap and Taz (Azzolin et al., 2014), our data suggest that the phenotypic differences observed between mutants obtained by using $Wnt1^{Cre}$ and $Wnt1^{Cre2SOR}$ may be caused by elevated Wnt signaling from the $Wnt1^{Cre}$ transgene (Chai et al., 2000).

Yap and *Taz* regulate vascular development

The diminished expression of CD31 in E10.5 *Yap* and *Taz* mutants indicated that *Yap* and *Taz* have an essential role in craniofacial vascular development. We found that the multipotent O9-1 NC cells treated with siRNAs targeting *Yap* and *Taz* were defective in their ability to differentiate into smooth muscle cells. Moreover, our RNA-Seq data revealed that genes functioning in adherens junction formation, endothelial cell migration, vasoconstriction, and the cytoskeleton were differentially expressed in *Yap* and *Taz* mutants, suggesting that other developmental events may also contribute to defective vascular development.

We noted that genes encoding the Jak-Stat cascade components, including *Jak3*, *Ptk2b*, *Stat3*, *Stat5a*, and *Stat5b*, were upregulated in *Wnt1*^{Cre}; *Yap*; *Taz* dCKO mutants. A previous study reported that the activation of *Stat3* promotes the apoptosis of vascular smooth muscle cells by triggering mitochondria mediated cell death receptors and cell death pathways (Bai et al., 2008). Further work is required to investigate the role of increased Jak-Stat pathway components during craniofacial development in an *in vivo* setting.

Prox1, a regulator of lymphatic development, transcripts were also elevated in *Yap* and *Taz* mutant embryos. Specification of lymphatic endothelial cells is an essential event in vascular development (Wigle and Oliver, 1999; Wigle et al., 2002; Johnson et al., 2008); thus, elevated *Prox1* levels may conceivably disrupt normal vascular specification. It will be interesting to determine in future experiments whether increased *Prox1* expression leads to fate switching to a predominantly lymphatic endothelial cell phenotype.

We found that *Pdgfb* is also upregulated in *Yap* and *Taz* mutant embryos. PDGF signaling has been implicated both directly and indirectly in the regulation of vasculogenesis and angiogenesis. Given the critical role of *Pdgfb* in regulating the recruitment and proliferation of vascular cells (Yancopoulos et al., 2000), the defective vascular development observed in *Yap* and *Taz* mutant embryos may be related to increased *Pdgfb* expression.

The Hippo pathway regulates CNC proliferation and apoptosis

We showed that proliferation was significantly reduced in the mandibular mesenchyme in *Yap* and *Taz* mutant embryos. This diminished proliferation is consistent with our observation of reduced cell density surrounding the enlarged vessels in *Yap* and *Taz* mutant embryos. Furthermore, a recent study showed that NC migration and fate specification were spared in *Wnt1*^{Cre}; *Yap*; *Taz* embryos at E10.5, suggesting that Yap and Taz regulate proliferation in the post migratory CNC (Manderfield et al., 2014). In *Wnt1*^{cre2SOR}; *Yap*; *Taz* embryos, we also found that proliferation was intact in the neural tube, despite the open neural tube phenotype, indicating that other mechanisms likely account for the failure of neural tube closure.

Consistent with our *in vivo* observations, we found that the siRNA-mediated knockdown of *Yap* and *Taz* significantly reduced the proliferation of multipotent NC O9-1 cells, further supporting that *Yap* and *Taz* are critical for NC cell proliferation. We also showed that the knockdown of *Lats1* and *Lats2* significantly increased the proliferation of O9-1 cells, which is consistent with the idea that Yap and Taz function as Hippo pathway effectors to regulate NC proliferation.

In addition, apoptosis was significantly increased in the mandibular mesenchyme in *Yap* and *Taz* mutant embryos. Both decreased proliferation and increased apoptosis were observed in E9.5 *Yap* and *Taz* mutant embryos in the absence of any detectable hemorrhage, indicating that the reduced cell proliferation and sparse cell density observed in E10.5 *Yap* and *Taz* mutant embryos were caused by a direct, primary effect of *Yap* and *Taz*, rather than a secondary effect due to the hemorrhaging.

The regulation of Fox genes by Yap and Taz and their potential roles in human disease

Fox transcription factors are key regulators of embryogenesis and control fundamental biological processes including cell proliferation, fate determination, differentiation, and growth (Kaufmann and Knochel, 1996; Kume et al., 1998; Kidson et al., 1999; Kume et al., 2001; Tuteja and Kaestner, 2007b; Tuteja and Kaestner, 2007a; Benayoun et al., 2011; Haldipur et al., 2014). Notably, Fox genes are evolutionarily and functionally conserved across multiple species, including mice and humans, making animal models invaluable tools for understanding the mechanisms underlying human diseases caused by Fox genes.

Expression of *Foxc1* was downregulated at the mRNA and protein level in *Yap* and *Taz* mutant embryos. Foxc1 has been implicated in several different human disorders including the most common cerebellar malformation, Dandy-Walker malformation (DWM); Axenfeld-Rieger syndrome (ARS); 6p25 deletion syndrome; and iridogoniodysgenesis (Mears et al., 1998; Nishimura et al., 1998; Maclean et al., 2005; Aldinger et al., 2009; Delahaye et al., 2012). In addition to the function of *Foxc1* in different diseases, it also has critical roles in the development of multiple organs and tissues including cerebellar, skull, ocular, and cardiovascular development (Kume, 2009). Notably, compound *Foxc1* and *Foxc2* knockout mouse embryo mutants have craniofacial abnormalities similar to those of *Yap*; *Taz* mutants, such as enlarged blood vessels, sparse mesenchyme, and an open neural tube (Kume et al., 2001).

Patients with mutations in *Foxc1* display a variant of the Dandy Walker malformation, including cerebellar vermis hypoplasia (CVH). Notably, *Foxc1* mutant mice also have an enlarged fourth ventricle roof plate. Similar to *Foxc1* mutant mice, *Yap*; *Taz* dCKO mice also display cerebellar hypoplasia with an enlarged fourth ventricle roof plate. In addition, *Foxc1* knockout mice are reported to have hydrocephalus (Kume et al., 1998), a severe and common lethal human birth defect, that was also observed in mice with *Yap* inactivation and *Taz* heterozygosity in NC cells. Collectively, these findings further support the hypothesis that Foxc1 is a downstream effector of Yap and Taz.

MATERIALS AND METHODS

Mouse alleles and transgenic lines

All animal experiments in this study were approved by the Baylor College of Medicine Institutional Review Board. The *Wnt1*^{Cre}, *Wnt1*^{Cre2SOR}, *Yap*$^{flox/+}$ and *Taz*$^{flox/+}$ mouse lines and alleles used in this study have been described previously (Chai et al., 2000; Xin et al., 2011; Lewis et al., 2013; Xin et al., 2013).

Histology and hematoxylin and eosin (H&E) staining

All embryos were dissected in phosphate-buffered saline (PBS) and fixed in 4% paraformaldehyde (PFA) overnight at 4°C. For H&E staining, the fixed embryos were dehydrated with an ethanol series (70% to 100%) and xylene and then embedded in paraffin. These tissues were subsequently cut into 7-μm sections and stained with H&E, as previously described (Lu et al., 1999).

O9-1 cell culture and siRNA knockdown

The O9-1 cells were cultured under undifferentiating conditions by following a previously published protocol (Ladher et al., 2000). The culture medium used consisted of Dulbecco's Modified Eagle's Medium supplemented with 15% fetal bovine serum, 0.1 mM MEM Nonessential Amino Acids, 1 mM sodium pyruvate, 55 μM β-mercaptoethanol, 100 units/mL penicillin/streptomycin, and 2 mM L-glutamine. Importantly, the medium was conditioned with growth-inhibited STO (Mouse embryonic fibroblast cell line) feeder cells overnight, filtered (0.22 μm pore size), and further supplemented with 25 ng/mL basic fibroblast growth factor (R&D Systems, Minneapolis, MN, 233-FB) and 1000 U leukemia inhibitory factor (EMD Millipore, Danvers, MA, ESG1106). The conditions used for smooth muscle differentiation were described previously (Ishii et al., 2012). For the siRNA knockdown experiments in O9-1 cells, siRNA SMARTpools targeting *Yap*, *Taz*, and Hippo kinases *Lats1* and *Lats2* were purchased from Dharmacon, Inc. (Lafayette, CO), and the transfections were performed by following a typical RNAiMAX transfection procedure (Thermo Fisher Scientific, Waltham, MA).

Yap exon 3 deletion by using CRISPR/Cas9

To make a *Yap* null O9-1 cell line, exon 3 of *Yap* was deleted using CRISPR/Cas9 genome editing. Two sgRNAs flanking exon 3 were identified using the sgRNA design tool (http://www.dna20.com). Four sgRNA oligonucleotides with overhanging BbsI restriction

sites were synthesized by IDT (Coralville, IA): 5'-CACCGtggattacgtgggtatgtt-3' (sgRNA1-forward), 5'-AAACaacatacccacgtaatccac-3' (sgRNA1-reverse), 5'-CACCGagatggtctaatgtagtga-3' (sgRNA2-forward), and 5'-AAACtcactacattagaccatctC-3' (sgRNA2-reverse). The paired oligonucleotides were annealed and ligated into a pSpCas9(bb)-2a-GFP vector (Addgene, Cambridge, MA, plasmid #48138). To create cell lines with a deletion of *Yap* exon 3, we transfected pSpCas9-GFP-YAP-sgRNA1 and pSpCas9-GFP-YAP-sgRNA2 into O9-1 cells using Lipofectamine 2000 (Thermo Fisher Scientific). Twenty-four hours after the transfection, the cells underwent fluorescence-activated cell sorting (FACS) with GFP/7-AAD. Viable, single cells ($7\text{-AAD}^{-};\text{GFP}^{+}$) were seeded into 96-well plates with culture medium. After 4-5 days, single colonies could be observed in some of the wells; wells that had more than one colony were excluded from further analyses. The single colonies were passaged into 12-well plates and incubated for 2-4 days to expand the clones. When the cells were more than 80% confluent, they were dissociated with trypsin and half of the sample was processed for DNA extraction while the other half was used to make a freezer stock culture. To detect the *Yap* exon 3 deletion, we designed PCR primers flanking the sgRNA recognition sites: 5'-AAAACAGTCTCCACTACCCCTT -3' (forward) and 5'-GGCCATCATAGATCCTGGACG-3' (reverse). Clones harboring a homozygous deletion for *Yap* exon 3 were retained and used for experimental analyses.

3D embryo imaging with optical projection tomography (OPT) microscopy

Optical projection tomography microscopy was used to determine embryonic craniofacial morphology. Specimens were embedded in 1% agarose (AMRESCO LLC, Solon, OH) and dehydrated in 25%, 50%, 75%, and 100% ethanol (Sigma-Aldrich, St. Louis, MO) for 2 hours each. Samples were then stored in fresh 100% ethanol overnight before clearing. The dehydrated samples were then completely cleared in BABB solution, which contained one part benzyl alcohol (Thermo Fisher Scientifics) and 2 parts benzyl benzoate (Acros Organics, Waltham, MA). Samples were then imaged on a home-build OPT system (BCM-OPT) (Singh et. al submitted) modified from a previous version (Wong et al., 2013). The BCM-OPT microscope consisted of an Optem Zoom 125C lens (Qioptiq, Waltham, MA) and an auxiliary objective lens attached to a Retiga 4000DC FAST 1394 CCD camera (QImaging, Surrey, BC) with a 1.38x TV tube (Qioptiq). Autofluorescence images of the embryos were acquired with an X-Cite illumination light source (EXFO, Quebec, QE) and both a 425/26 nm BrightLine bandpass excitation filter and a 520/20 nm emission filter (Semrock, Rochester,

NY). The embryos were rotated 360 degrees, with each view taken with a 0.3-degree step size. Acquired images were reconstructed by using NRecon Reconstruction software, and 3D rendering was performed by using CTVox software (Bruker Corporation, Camarillo, CA).

Immunofluorescence and immunohistochemistry

After the embryos were fixed overnight in 4% PFA and dehydrated, they were embedded in paraffin, cut into 7-µm sections, and collected on Superfrost Plus slides (Fisher Scientific, Pittsburgh, PA). The sections were rehydrated using xylene and a graded ethanol series to a final concentration of 70% and then processed for antigen retrieval.

For the immunofluorescence analysis, the antigens were retrieved by incubating the slides in citrate buffer (10 mM) for 2 minutes in a microwave oven. Nuclei were stained with 4,6-diamidino-2-phenylindole (DAPI) at a 1:500 dilution. Primary antibodies against phospho-histone H3 (Cell Signaling Technology, Inc., Danvers, MA) and FoxC1 (Abcam, Cambridge, MA) were used at a 1:200 dilution. A broad HRP-conjugated secondary antibody (Invitrogen) was used according to the manufacturer's guidelines. An anti-SMA-Cy3 antibody (Sigma-Aldrich, Clone 1A4) was used at a 1:200 dilution. Staining was then visualized by using a TSA Plus Fluorescence System (PerkinElmer, Boston, MA) and a Zeiss LSM 510 confocal microscope.

For the immunohistochemistry analysis, the antigens were retrieved by boiling the sections in ethylenediaminetetraacetic acid for 15 minutes, and then the tissues were permeabilized by incubating the sections with 0.5% triton X-100 for 15 minutes. Afterwards, the sections were treated with 0.3% H_2O_2 for 15 minutes and blocked with 10% donkey serum for 1 hour. The sections were incubated with primary antibody against FoxC1 (Novus Biologicals, Littleton, CO) at a 1:200 dilution overnight at 4°C. The next day, the sections were incubated with HRP-conjugated anti-goat IgG antibody (1:200 dilution) for 1 hour and then developed with DAB substrate (Vector Laboratories, Inc., Burlingame, CA) for 2 minutes and 30 seconds. Sections were subsequently washed with H_2O, stained with hematoxylin for 3 minutes, and then washed with H_2O again for 5 minutes. Then, they were dehydrated with an ethanol series to a final concentration of 100% and xylene and mounted.

Whole mount immunohistochemistry

E10.5 embryos were processed as described (Wythe et al., 2013). Briefly, the embryos were fixed in 4% PFA overnight, serially dehydrated to absolute methanol, bleached in 5% H_2O_2 / 95% methanol overnight, and rehydrated to PBS-Tween (0.1%). The embryos were blocked

for 2 hours (PBS / 5% goat serum / 0.5% Triton X-100), then incubated with an anti-CD31 antibody (MEC13.3, BD Biosciences, San Jose, CA, 1:200 dilution) in blocking solution for 3 days. The embryos were then washed and incubated with biotin-conjugated goat anti-rat IgG secondary antibody (Vector Laboratories, Inc., 1:250 dilution) for 2 days. The signal was amplified with Alexa Fluor 488 Tyramide (Thermo Fisher Scientific, T20948). The embryos were then washed in blocking solution and incubated with anti-SMA-Cy3 antibody (Sigma-Aldrich, Clone 1A4, 1:200 dilution) for 3 days at 4°C. After washing, the embryos were cleared in Sca*l*eA2 (Hama H et al., 2011, Nature Neuroscience) for 2 days, Sca*l*eB4 for 2 days, then embedded in 1% agarose in ddH_2O, and cleared for another 2 days in Sca*l*eA2. The embryos were then imaged on a Lightsheet Z.1 (Zeiss) using a 5X air lens (NA=0.16) in Sca*l*eA2. All images were obtained using the same laser power and exposure time. Serial images were aligned using Zen software (Zeiss, Irvine, CA), and 3D rendering was performed with Imaris software (Bitplane USA, Concord, MA).

RNA-Seq and data analysis

Mandibular tissues from *Wnt1*^{cre}, *Yap*, and *Taz* dCKO mutant and control E10.5 embryos were dissected in diethylpyrocarbonate-treated PBS. Total RNA extracted from these tissues was treated with RNAse free DNase I (Ambion) for 30 min at 37°C. Then, the poly(A) RNA was purified with the MicroPoly(A) Purist Kit according to the manufacturer's instructions (Thermo Fisher Scientific). The purified RNA samples were processed for cDNA synthesis and library preparation. cDNA sequencing using the Illumina platform and read mapping were performed as previously described (Nagalakshmi et al., 2008). Datasets were processed for gene ontology analysis, which provided different terms that represent gene properties including cellular components, molecular function, and biological processes. The data were deposited in the Gene Expression Omnibus (GEO) database (accession no. GSE69311). More information is available at http://www.ncbi.nlm.nih.gov/geo/query/acc.cgi?token=ejajwkiynvevjuj&acc=GSE69311.

Chromatin immunoprecipitation (ChIP)

Embryonic orofacial tissues from wild type mice at stages E10.5-E11.5 were dissected for Yap ChIP analysis, as previously described (Wang et al., 2013). Normal rabbit IgG was used as a replacement control for the anti-Yap ChIP assay to show nonspecific immunoprecipitation of the chromatin. The primers used to amplify the TEAD regulatory element in the 5′ upstream region of the *Foxc1* genomic sequence were 5′-

CCTTGGCATCTCTCAGAAAGTC -3′ (sense) and 5′- TAGTCCTATCCCAGTGAGCATC -3′ (antisense).

Real-time PCR

For the real-time RT-PCR analysis, total RNA was isolated from the mandibles of E10.5 embryos or O9-1 cells by using the RNeasy Micro Kit (Qiagen) and processed for cDNA synthesis using Super Script II Reverse Transcriptase (Invitrogen). For the real-time ChIP-PCR analysis, immunoprecipitated DNA and input DNA were used as templates. All real-time thermal cycling was performed with the StepOne Real-time PCR System (Thermo Fisher Scientific). SYBR Green JumpStart Taq ReadyMix (Sigma-Aldrich) was used for real-time thermal cycling. All error bars represent SEM.

Cell counts and data analyses

For embryonic cell counting, all embryos used were at the same embryonic stage. The embryos were embedded carefully to maintain the same orientation and were sectioned at identical thickness (5 μm). Sections were carefully chosen to represent the matching regions between control and mutant embryos. Our analyses included at least 3 embryos for each genotype. For O9-1 cell counting, each experiment was performed in duplicate and all experiments were repeated 3 times or more. Image J software (National Institutes of Health, Bethesda, MD) was used to perform the cell counting and over 200 cells was counted for each experiment. The percentage of proliferating cells was determined by counting the pHH3-positive cells and dividing that number by the number of DAPI-positive cells. The percentage of apoptotic cells was determined by counting the number of TUNEL-positive cells. All counting data are represented in graphs as the mean ± SEM. The 2-tailed t-test was used to determine statistical significance, and $P<0.05$ was considered statistically significant.

Acknowledgments

We thank Dr. Nicole Stancel and Heather Leibrecht for editorial assistance in the preparation of the manuscript. We also thank Matthew C. Hill for Tead binding site analysis and Alan Chen for cell counting.

Competing interests

No competing interests declared.

Author contributions

J.W. and J.F.M. designed research; J.W., X.Y, C.W.H, I.M.M, Y.B. and J.D.W. performed research; J.W., X.Y, C.W.H, I.M.M, M.Z., J.D.W. M.E.D. and J.F.M. analyzed data; M. I., R.E.M and E.N.O provided reagents; J.W., C.W.H, J.D.W. and J.F.M. wrote the manuscript.

Funding

This work was supported by American Heart Association (AHA) National Center Scientist Development Grant (SDG) 14SDG19840000 (to J.W.), 2014 Lawrence Research Award from the Rolanette and Berdon Lawrence Bone Disease Program of Texas (to J.W.),. AHA National Center SDG 12SDG (to J. D. W.), NIH 2T32GM088129-06 (to IMMT), NIH R01HL118761 and R01DE023177 (to J.F.M.), and the Vivian L. Smith foundation (to J.F.M.). J.F.M was supported by Transatlantic Network of Excellence Award LeDucq Foundation Transatlantic Networks of Excellence in Cardiovascular Research 14CVD01: "Defining the genomic topology of atrial fibrillation." Also supported by Baylor College of Medicine IDDRC Grant Number 1 U54 HD083092 from the Eunice Kennedy Shriver National Institute of Child Health & Human Development and the Mouse Phenotyping Core at Baylor College of Medicine with funding from the NIH (U54 HG006348).

REFERENCES

Acloque, H., Adams, M. S., Fishwick, K., Bronner-Fraser, M. and Nieto, M. A. (2009) 'Epithelial-mesenchymal transitions: the importance of changing cell state in development and disease', *J Clin Invest* 119(6): 1438-49.

Aldinger, K. A., Lehmann, O. J., Hudgins, L., Chizhikov, V. V., Bassuk, A. G., Ades, L. C., Krantz, I. D., Dobyns, W. B. and Millen, K. J. (2009) 'FOXC1 is required for normal cerebellar development and is a major contributor to chromosome 6p25.3 Dandy-Walker malformation', *Nature Genetics* 41(9): 1037-42.

Azzolin, L., Panciera, T., Soligo, S., Enzo, E., Bicciato, S., Dupont, S., Bresolin, S., Frasson, C., Basso, G., Guzzardo, V. et al. (2014) 'YAP/TAZ incorporation in the beta-catenin destruction complex orchestrates the Wnt response', *Cell* 158(1): 157-70.

Bai, Y., Ahmad, U., Wang, Y., Li, J. H., Choy, J. C., Kim, R. W., Kirkiles-Smith, N., Maher, S. E., Karras, J. G., Bennett, C. F. et al. (2008) 'Interferon-gamma induces X-linked inhibitor of apoptosis-associated factor-1 and Noxa expression and potentiates human vascular smooth muscle cell apoptosis by STAT3 activation', *Journal of Biological Chemistry* 283(11): 6832-42.

Benayoun, B. A., Caburet, S. and Veitia, R. A. (2011) 'Forkhead transcription factors: key players in health and disease', *Trends in Genetics* 27(6): 224-32.

Carmona-Fontaine, C., Matthews, H. K., Kuriyama, S., Moreno, M., Dunn, G. A., Parsons, M., Stern, C. D. and Mayor, R. (2008) 'Contact inhibition of locomotion in vivo controls neural crest directional migration', *Nature* 456(7224): 957-61.

Chai, Y., Jiang, X., Ito, Y., Bringas, P., Jr., Han, J., Rowitch, D. H., Soriano, P., McMahon, A. P. and Sucov, H. M. (2000) 'Fate of the mammalian cranial neural crest during tooth and mandibular morphogenesis', *Development* 127(8): 1671-9.

Coles, E., Christiansen, J., Economou, A., Bronner-Fraser, M. and Wilkinson, D. G. (2004) 'A vertebrate crossveinless 2 homologue modulates BMP activity and neural crest cell migration', *Development* 131(21): 5309-17.

Cordero, D. R., Brugmann, S., Chu, Y., Bajpai, R., Jame, M. and Helms, J. A. (2011) 'Cranial neural crest cells on the move: their roles in craniofacial development', *Am J Med Genet A* 155A(2): 270-9.

Delahaye, A., Khung-Savatovsky, S., Aboura, A., Guimiot, F., Drunat, S., Alessandri, J. L., Gerard, M., Bitoun, P., Boumendil, J., Robin, S. et al. (2012) 'Pre- and postnatal phenotype of 6p25 deletions involving the FOXC1 gene', *American Journal of Medical Genetics. Part A* 158A(10): 2430-8.

Garcia-Castro, M. I., Marcelle, C. and Bronner-Fraser, M. (2002) 'Ectodermal Wnt function as a neural crest inducer', *Science* 297(5582): 848-51.

Glavic, A., Silva, F., Aybar, M. J., Bastidas, F. and Mayor, R. (2004) 'Interplay between Notch signaling and the homeoprotein Xiro1 is required for neural crest induction in Xenopus embryos', *Development* 131(2): 347-59.

Haldipur, P., Gillies, G. S., Janson, O. K., Chizhikov, V. V., Mithal, D. S., Miller, R. J. and Millen, K. J. (2014) 'Foxc1 dependent mesenchymal signalling drives embryonic cerebellar growth', *Elife* 3.

Heallen, T., Zhang, M., Wang, J., Bonilla-Claudio, M., Klysik, E., Johnson, R. L. and Martin, J. F. (2011) 'Hippo pathway inhibits Wnt signaling to restrain cardiomyocyte proliferation and heart size', *Science* 332(6028): 458-61.

Ishii, M., Arias, A. C., Liu, L., Chen, Y. B., Bronner, M. E. and Maxson, R. E. (2012) 'A stable cranial neural crest cell line from mouse', *Stem Cells and Development* 21(17): 3069-80.

Johnson, N. C., Dillard, M. E., Baluk, P., McDonald, D. M., Harvey, N. L., Frase, S. L. and Oliver, G. (2008) 'Lymphatic endothelial cell identity is reversible and its maintenance requires Prox1 activity', *Genes and Development* 22(23): 3282-91.
Kaufmann, E. and Knochel, W. (1996) 'Five years on the wings of fork head', *Mechanisms of Development* 57(1): 3-20.
Kidson, S. H., Kume, T., Deng, K., Winfrey, V. and Hogan, B. L. (1999) 'The forkhead/winged-helix gene, Mf1, is necessary for the normal development of the cornea and formation of the anterior chamber in the mouse eye', *Dev Biol* 211(2): 306-22.
Kume, T. (2009) 'The cooperative roles of Foxc1 and Foxc2 in cardiovascular development', *Advances in Experimental Medicine and Biology* 665: 63-77.
Kume, T., Deng, K. Y., Winfrey, V., Gould, D. B., Walter, M. A. and Hogan, B. L. (1998) 'The forkhead/winged helix gene Mf1 is disrupted in the pleiotropic mouse mutation congenital hydrocephalus', *Cell* 93(6): 985-96.
Kume, T., Jiang, H., Topczewska, J. M. and Hogan, B. L. (2001) 'The murine winged helix transcription factors, Foxc1 and Foxc2, are both required for cardiovascular development and somitogenesis', *Genes and Development* 15(18): 2470-82.
Ladher, R. K., Church, V. L., Allen, S., Robson, L., Abdelfattah, A., Brown, N. A., Hattersley, G., Rosen, V., Luyten, F. P., Dale, L. et al. (2000) 'Cloning and expression of the Wnt antagonists Sfrp-2 and Frzb during chick development', *Developmental Biology* 218(2): 183-98.
Lewis, A. E., Vasudevan, H. N., O'Neill, A. K., Soriano, P. and Bush, J. O. (2013) 'The widely used Wnt1-Cre transgene causes developmental phenotypes by ectopic activation of Wnt signaling', *Dev Biol* 379(2): 229-34.
Lindahl, P., Johansson, B. R., Leveen, P. and Betsholtz, C. (1997) 'Pericyte loss and microaneurysm formation in PDGF-B-deficient mice', *Science* 277(5323): 242-5.
Lu, M. F., Pressman, C., Dyer, R., Johnson, R. L. and Martin, J. F. (1999) 'Function of Rieger syndrome gene in left-right asymmetry and craniofacial development', *Nature* 401(6750): 276-8.
Maclean, K., Smith, J., St Heaps, L., Chia, N., Williams, R., Peters, G. B., Onikul, E., McCrossin, T., Lehmann, O. J. and Ades, L. C. (2005) 'Axenfeld-Rieger malformation and distinctive facial features: Clues to a recognizable 6p25 microdeletion syndrome', *American Journal of Medical Genetics. Part A* 132A(4): 381-5.
Manderfield, L. J., Aghajanian, H., Engleka, K. A., Lim, L. Y., Liu, F., Jain, R., Li, L., Olson, E. N. and Epstein, J. A. (2015) 'Hippo signaling is required for Notch-dependent smooth muscle differentiation of neural crest', *Development* 142(17): 2962-71.
Manderfield, L. J., Engleka, K. A., Aghajanian, H., Gupta, M., Yang, S., Li, L., Baggs, J. E., Hogenesch, J. B., Olson, E. N. and Epstein, J. A. (2014) 'Pax3 and hippo signaling coordinate melanocyte gene expression in neural crest', *Cell Rep* 9(5): 1885-95.
Mears, A. J., Jordan, T., Mirzayans, F., Dubois, S., Kume, T., Parlee, M., Ritch, R., Koop, B., Kuo, W. L., Collins, C. et al. (1998) 'Mutations of the forkhead/winged-helix gene, FKHL7, in patients with Axenfeld-Rieger anomaly', *American Journal of Human Genetics* 63(5): 1316-28.
Moreno, L. M., Mansilla, M. A., Bullard, S. A., Cooper, M. E., Busch, T. D., Machida, J., Johnson, M. K., Brauer, D., Krahn, K., Daack-Hirsch, S. et al. (2009) 'FOXE1 association with both isolated cleft lip with or without cleft palate, and isolated cleft palate', *Human Molecular Genetics* 18(24): 4879-96.
Morikawa, Y., Zhang, M., Heallen, T., Leach, J., Tao, G., Xiao, Y., Bai, Y., Li, W., Willerson, J. T. and Martin, J. F. (2015) 'Actin cytoskeletal remodeling with protrusion formation is essential for heart regeneration in Hippo-deficient mice', *Sci Signal* 8(375): ra41.

Nagalakshmi, U., Wang, Z., Waern, K., Shou, C., Raha, D., Gerstein, M. and Snyder, M. (2008) 'The transcriptional landscape of the yeast genome defined by RNA sequencing', *Science* 320(5881): 1344-9.
Nishimura, D. Y., Swiderski, R. E., Alward, W. L., Searby, C. C., Patil, S. R., Bennet, S. R., Kanis, A. B., Gastier, J. M., Stone, E. M. and Sheffield, V. C. (1998) 'The forkhead transcription factor gene FKHL7 is responsible for glaucoma phenotypes which map to 6p25', *Nature Genetics* 19(2): 140-7.
Prescott, S. L., Srinivasan, R., Marchetto, M. C., Grishina, I., Narvaiza, I., Selleri, L., Gage, F. H., Swigut, T. and Wysocka, J. (2015) 'Enhancer divergence and cis-regulatory evolution in the human and chimp neural crest', *Cell* 163(1): 68-83.
Santagati, F. and Rijli, F. M. (2003) 'Cranial neural crest and the building of the vertebrate head', *Nat Rev Neurosci* 4(10): 806-18.
Sauka-Spengler, T. and Bronner-Fraser, M. (2008) 'A gene regulatory network orchestrates neural crest formation', *Nat Rev Mol Cell Biol* 9(7): 557-68.
Sela-Donenfeld, D. and Kalcheim, C. (1999) 'Regulation of the onset of neural crest migration by coordinated activity of BMP4 and Noggin in the dorsal neural tube', *Development* 126(21): 4749-62.
Tuteja, G. and Kaestner, K. H. (2007a) 'Forkhead transcription factors II', *Cell* 131(1): 192.
Tuteja, G. and Kaestner, K. H. (2007b) 'SnapShot: forkhead transcription factors I', *Cell* 130(6): 1160.
Wang, J., Bai, Y., Li, H., Greene, S. B., Klysik, E., Yu, W., Schwartz, R. J., Williams, T. J. and Martin, J. F. (2013) 'MicroRNA-17-92, a direct Ap-2alpha transcriptional target, modulates T-box factor activity in orofacial clefting', *PLoS Genet* 9(9): e1003785.
Wigle, J. T., Harvey, N., Detmar, M., Lagutina, I., Grosveld, G., Gunn, M. D., Jackson, D. G. and Oliver, G. (2002) 'An essential role for Prox1 in the induction of the lymphatic endothelial cell phenotype', *EMBO Journal* 21(7): 1505-13.
Wigle, J. T. and Oliver, G. (1999) 'Prox1 function is required for the development of the murine lymphatic system', *Cell* 98(6): 769-78.
Williamson, K. A., Rainger, J., Floyd, J. A., Ansari, M., Meynert, A., Aldridge, K. V., Rainger, J. K., Anderson, C. A., Moore, A. T., Hurles, M. E. et al. (2014) 'Heterozygous loss-of-function mutations in YAP1 cause both isolated and syndromic optic fissure closure defects', *American Journal of Human Genetics* 94(2): 295-302.
Wong, M. D., Dazai, J., Walls, J. R., Gale, N. W. and Henkelman, R. M. (2013) 'Design and implementation of a custom built optical projection tomography system', *PLoS One* 8(9): e73491.
Wythe, J. D., Dang, L. T., Devine, W. P., Boudreau, E., Artap, S. T., He, D., Schachterle, W., Stainier, D. Y., Oettgen, P., Black, B. L. et al. (2013) 'ETS factors regulate Vegf-dependent arterial specification', *Developmental Cell* 26(1): 45-58.
Xin, M., Kim, Y., Sutherland, L. B., Murakami, M., Qi, X., McAnally, J., Porrello, E. R., Mahmoud, A. I., Tan, W., Shelton, J. M. et al. (2013) 'Hippo pathway effector Yap promotes cardiac regeneration', *Proc Natl Acad Sci U S A* 110(34): 13839-44.
Xin, M., Kim, Y., Sutherland, L. B., Qi, X., McAnally, J., Schwartz, R. J., Richardson, J. A., Bassel-Duby, R. and Olson, E. N. (2011) 'Regulation of insulin-like growth factor signaling by Yap governs cardiomyocyte proliferation and embryonic heart size', *Sci Signal* 4(196): ra70.
Yancopoulos, G. D., Davis, S., Gale, N. W., Rudge, J. S., Wiegand, S. J. and Holash, J. (2000) 'Vascular-specific growth factors and blood vessel formation', *Nature* 407(6801): 242-8.

Figures

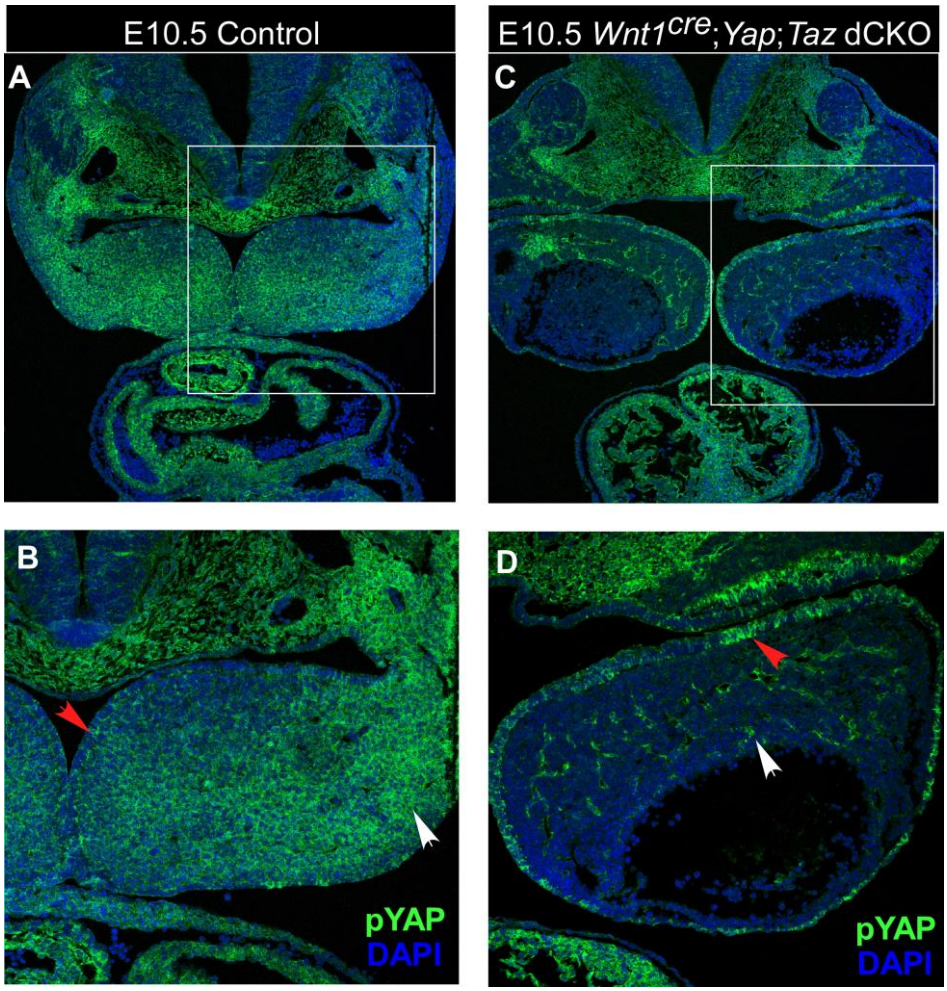

Fig. 1. Efficient deletion of *Yap* and *Taz* in CNC-derived cells. Hippo signaling activity, indicated by the level of phosphorylated Yap (pYAP), is shown in control embryos (A-B) and in *Wnt1*^{Cre}; *Yap*$^{f/f}$;*Taz*$^{f/f}$ embryos (C-D). pYAP levels were reduced in CNC-derived cells (white arrows) but not in non-CNC derived cells (red arrows). Hippo-active cells (green) were stained with pYAP; nuclei (blue) were stained with DAPI.

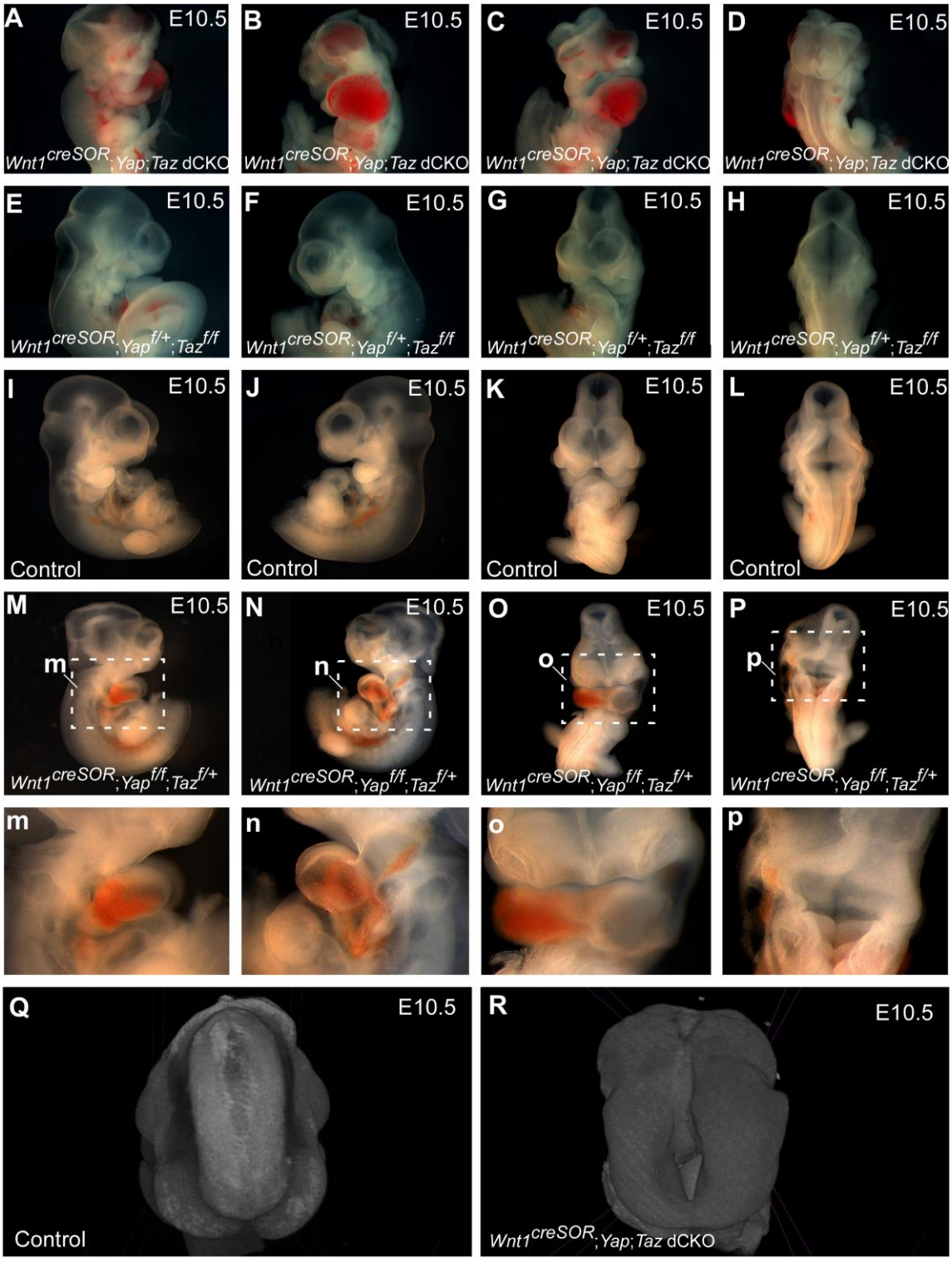

Fig. 2. Vascular defects, hemorrhage, and neural tube defects following *Yap* and *Taz* inactivation using the *Wnt1*^{Cre2SOR} Cre driver. Both *Wnt1*^{Cre2SOR}; *Yap*; *Taz* dCKO (A-D) and *Wnt1*^{Cre2SOR}; *Yap*$^{f/f}$; *Taz*$^{f/+}$ (M-P) embryos showed lethality at E10.5 with severe vascular

defects, hemorrhage, and defects in neural tube closure, whereas control embryos (I-L) and *Wnt1*^{Cre2SOR}; *Yap*$^{f/+}$; *Taz*$^{f/f}$ embryos (E-H) showed no obvious defects. Zoomed-in images of branchial arch vessel defects, hemorrhage, and neural tube defects of *Wnt1*^{Cre2SOR}; *Yap*$^{f/f}$; *Taz*$^{f/+}$ embryos are shown (m-p). Three dimensional imaging using optical projection tomography microscopy indicated that the neural tube of control embryos closed normally (Q), whereas *Wnt1*^{Cre2SOR}; *Yap*; *Taz* dCKO embryos had a defect in neural tube closure (R).

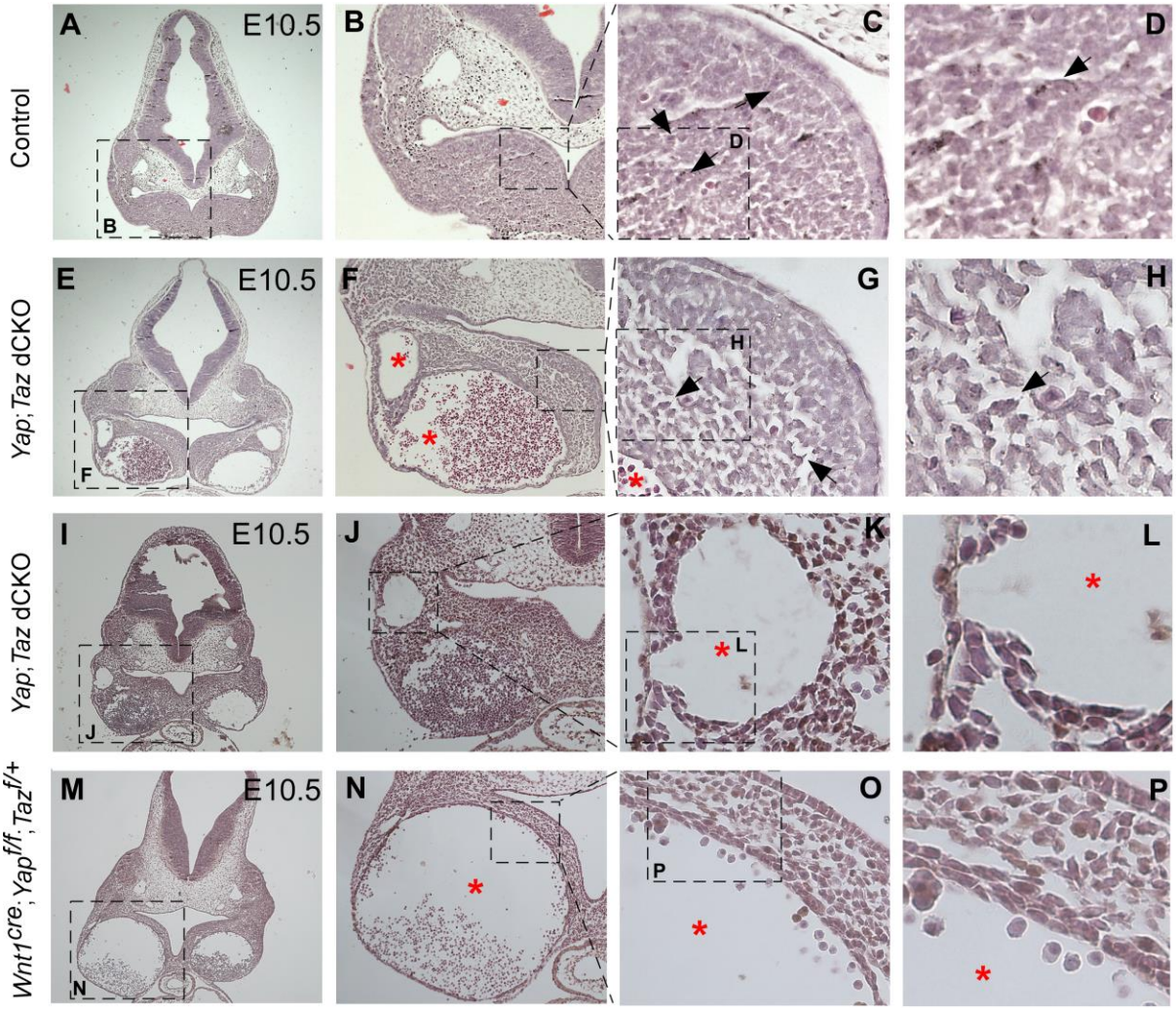

Fig. 3. Histologic analysis showing the disruption of mandibular structure in *Yap* and *Taz*–deficient embryos. Coronal sections stained with hematoxylin and eosin showing that, in contrast to control embryos (A-D), both *Wnt1*^{Cre}; *Yap*; *Taz* dCKO (E-L) and *Wnt1*^{Cre}; *Yap*$^{f/f}$; *Taz*$^{f/+}$ (M-P) embryos had disorganized, sparse mesenchyme (black arrows) and enlarged vessels (red stars) in the mandible. Boxed areas are shown at higher magnification in panels to the right, as labeled.

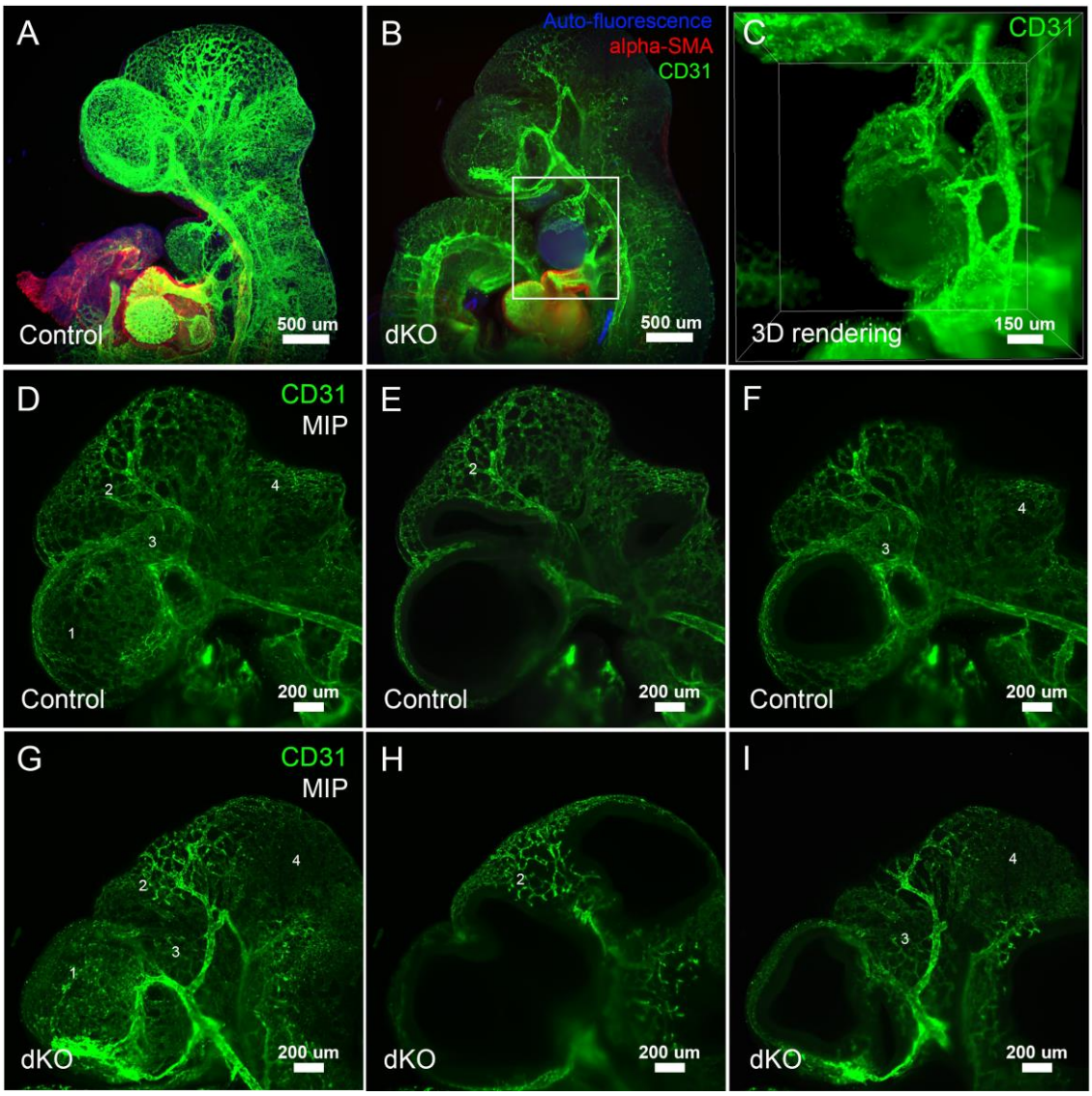

Fig. 4. Severe vessel defects caused by *Yap* and *Taz* deletion. Whole mount CD31 immunofluorescence staining in a control (A) and a *Wnt1*^{Cre}; *Yap*; *Taz* dCKO mutant (B) revealed vessel defects and endothelial-lined hemangiomas in the forebrain and mandible in *Wnt1*^{Cre}; *Yap*; *Taz* dCKO mutants (B). The boxed area in B is shown at a higher magnification in C, focusing in on the endothelial-lined hemangiomas in the branchial arch in the *Yap*; *Taz* dCKO embryo (C). Whereas control embryos had normal vessel development in brain (D-F), *Wnt1*^{Cre}; *Yap*; *Taz* dCKO mutants had vessel regression and disorganization (different regions are labeled as 1-4). (G-I). Endothelial cells (green) are stained with CD31 antibody; smooth muscle cells (red) are stained with SMA antibody; and auto fluorescence is shown in blue.

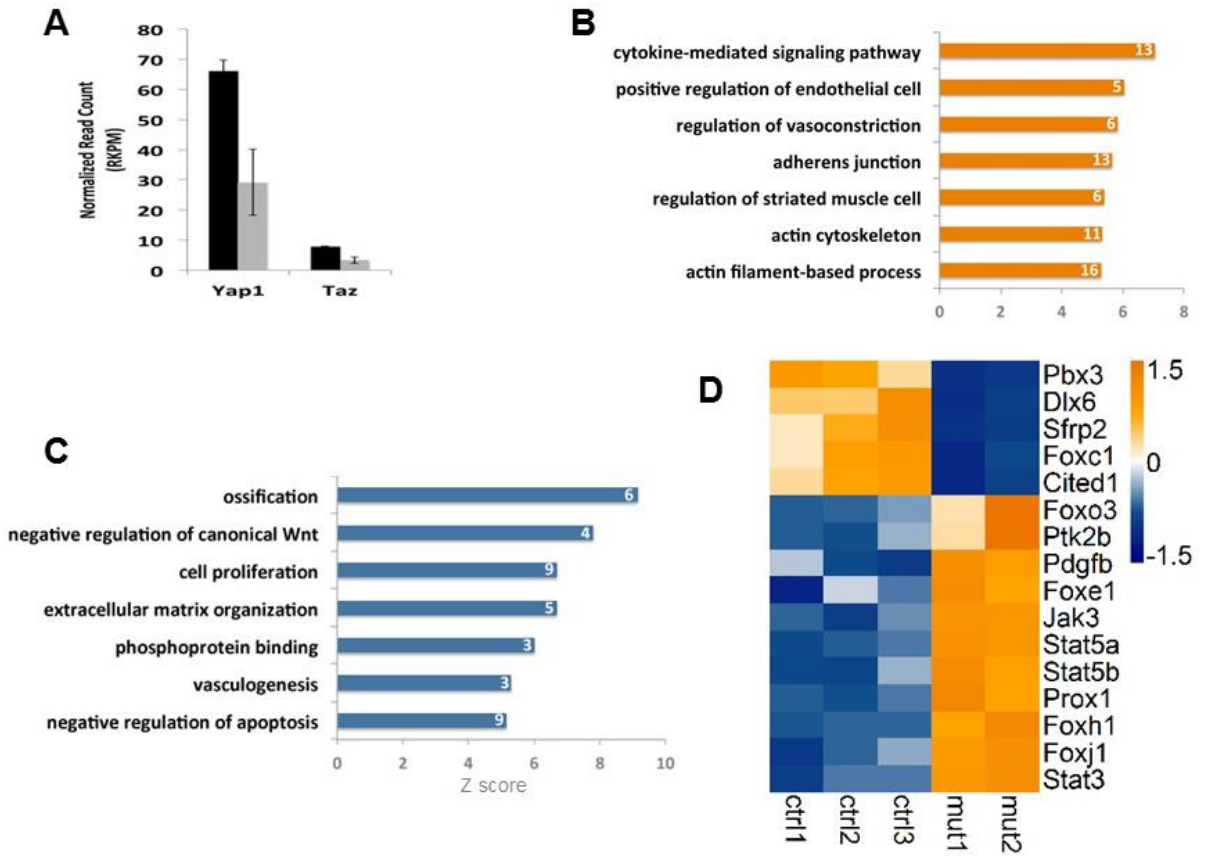

Fig. 5. The regulation of multiple signals by the Hippo pathway in CNC-derived cells. RNA-Seq analysis was performed by using mandibular tissues from E10.5 control embryos and *Wnt1*^{Cre} *Taz; Yap* dKO mutants. (A) RNA-Seq analysis indicates that *Yap* and *Taz* expression levels (indicated by reads) were decreased by 40% to 50% in *Wnt1*^{Cre} *Taz; Yap* dKO embryos compared to control embryos. (B) Gene ontology analysis shows genes that are upregulated in *Wnt1*^{Cre} *Taz; Yap* dKO embryos compared to control embryos, which includes genes that regulate adherens junctions, vasoconstriction, and the cytoskeleton. (C) Gene ontology analysis shows genes that are downregulated in *Wnt1*^{Cre} *Taz; Yap* dKO embryos compared to control embryos, which includes genes that regulate cell proliferation and vasculogenesis and that negatively regulate canonical Wnt. (D) Heat map of RNA-Seq data shows that, compared to controls, *Wnt1*^{Cre} *Taz; Yap* dKO mutants had downregulated expression of *Foxc1* and upregulated expression of *Foxe1, Prox1 , Pdgfb,* and Jak-Stat genes including *Jak3, Ptk2b, Stat3, Stat5a,* and *Stat5b*.

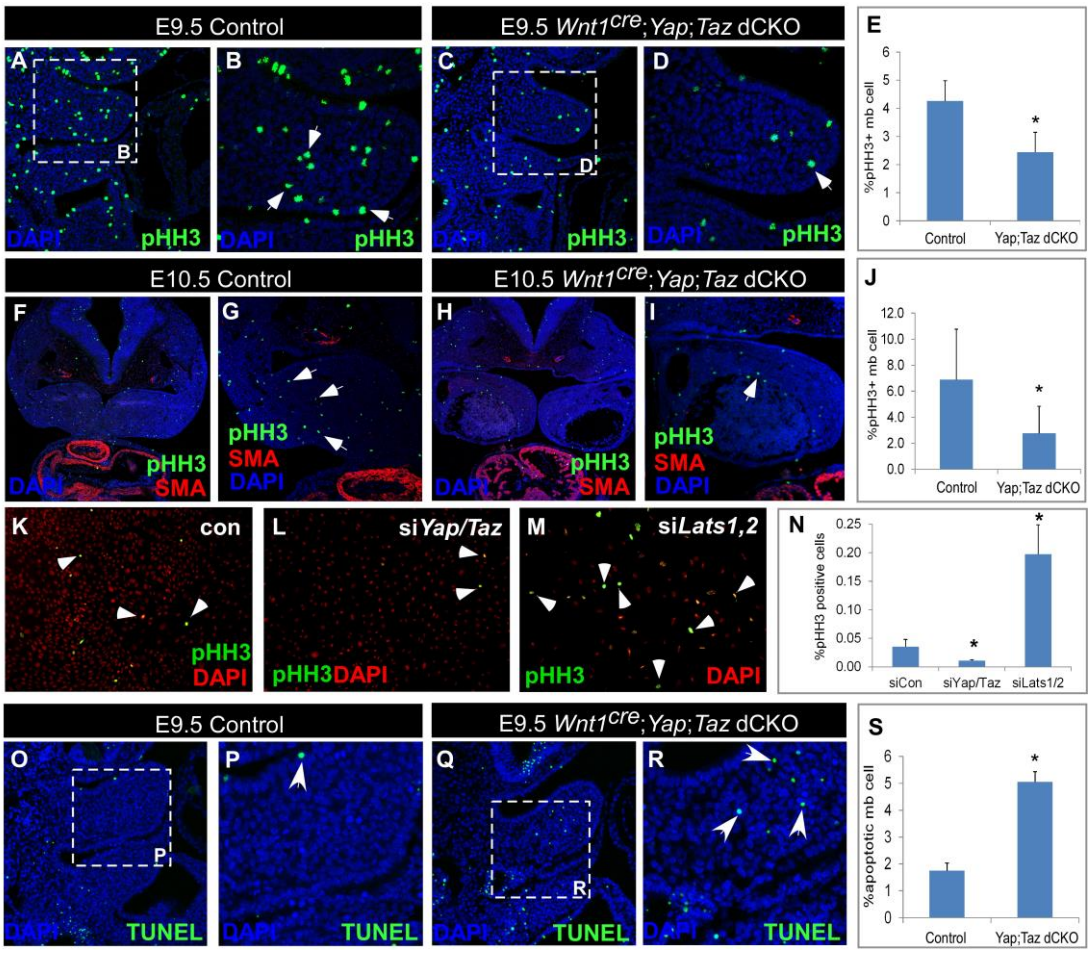

Fig. 6. The regulation of proliferation and apoptosis in CNC cells by the Hippo pathway. Compared to control embryos, *Wnt1*^{Cre}; *Yap*; *Taz* dCKO embryos had a significantly diminished percentage of pHH3-positive proliferating cells in the mandible at E9.5 and E10.5 (A-J). Proliferating cells (green) were stained with pHH3 antibody; smooth muscle cells (red) were stained with SMA antibody; and nuclei (blue) were stained with DAPI. *p<0.05. (K-N) Compared to O9-1 cells transfected with control (con) siRNA, O9-1 cells transfected with *Yap* and *Taz* siRNA had significantly reduced proliferation, and O9-1 cells transfected with *Lats1* and *Lats2* siRNA had significantly increased proliferation (*p<0.05). Proliferating cells (green) were stained with pHH3 antibody; nuclei (red) were stained with DAPI. (O-S) Compared to control embryos, *Wnt1*^{Cre}; *Yap*; *Taz* dCKO embryos had a significantly increased percentage of apoptotic cells in the mandible at E9.5 (*p<0.05). Apoptotic cells (green) were stained with TUNEL; nuclei (blue) were stained with DAPI. All error bars represent SEM.

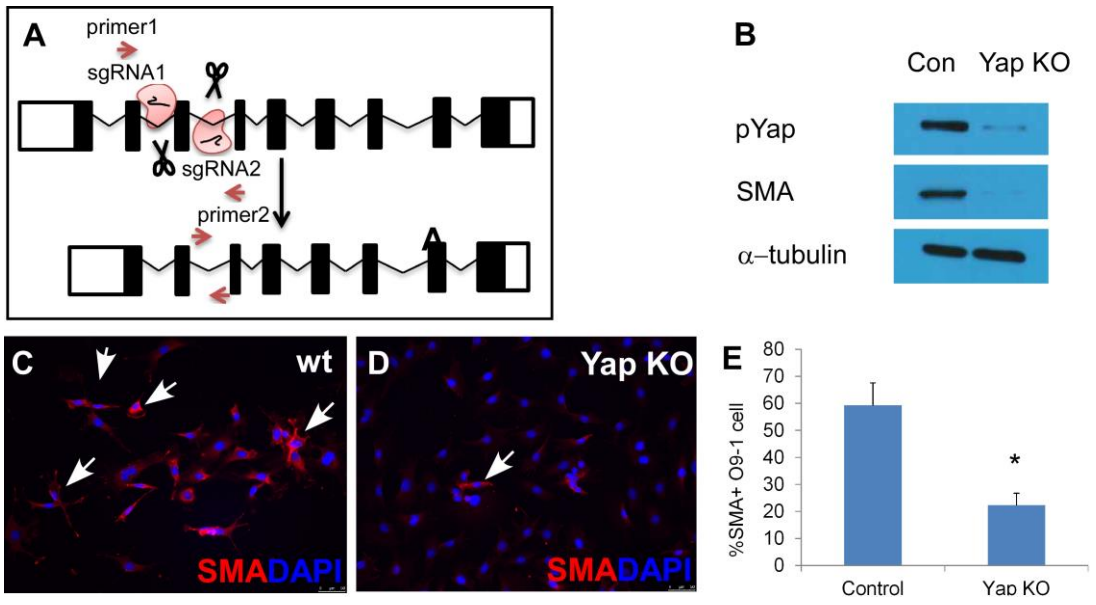

Fig. 7. The requirement of *Yap* for smooth muscle differentiation. The strategy for establishing a *Yap* knockout (KO) O9-1 cell line by using CRISPR/Cas9 system (A). Specifically, exon 3 was deleted from *Yap*. Western blot data shows diminished SMA and pYap expression in *Yap* KO O9-1 cells compared to wild type (wt) O9-1 cells (B). Under differentiation conditions, most wild type O9-1 cells give rise to smooth muscle cells (C), whereas *Yap* KO O9-1 cells did not give rise to smooth muscle cells (D) Arrows designate SMA positive cells. Cell counting data show that the percentage of SMA-positive cells was significantly reduced in *Yap* KO O9-1 cells compared to wild type O9-1 cells (*$p<0.01$). Error bars represent SEM. (E). Smooth muscle cells (red) were stained with SMA antibody; nuclei (blue) were stained with DAPI.

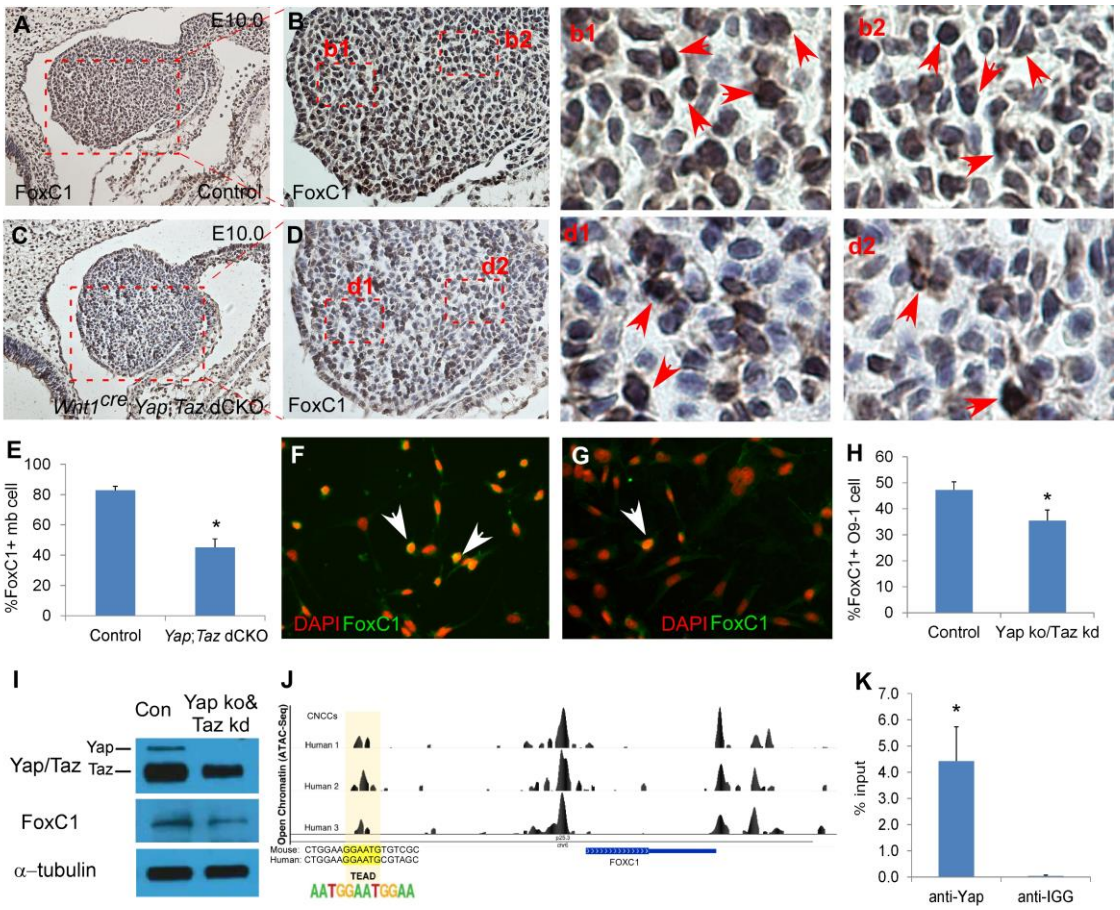

Fig. 8. The regulation of *Foxc1* by Yap and Taz. Immunohistochemical staining of Foxc1 in sagittal sections of the mandible show that the majority of cells in control embryos express *Foxc1* (A-B, b1-b2), whereas the expression of Foxc1 was diminished in *Wnt1*^{Cre}; *Yap*; *Taz* dCKO embryos (C-D, d1-d2). Boxed areas are shown at higher magnification in panels to the right, as labeled. Cell counting data show that the percentage of cells positive for Foxc1 expression in the mandible was significantly reduced in *Wnt1*^{Cre}; *Yap*; *Taz* dCKO embryos compared to control embryos (E) (*$p<0.01$). Immunohistochemical staining of Foxc1 in O9-1 cells shows significantly decreased Foxc1 expression in *Yap* knockout (KO); *Taz* knockdown (KD) O9-1 cells compared to wild-type O9-1 cells (*$p<0.05$) (F-H). Arrows designate Foxc1 positive cells. Western blot analysis of Foxc1 in O9-1 cells shows decreased Foxc1 expression in response to decreased Yap and Taz expression level (I). (J) Conserved Tead binding site located in the upstream region of *FOXC1*. Peaks in ATAC-seq data (accession no. GSE70751) indicated chromatin accessibility (Prescott et al., 2015). (K) In vivo real-time PCR using ChIP DNA indicates that *Foxc1* was bound by the Yap-Tead complex in embryonic facial tissue. $p<0.05$. All error bars represent SEM.